Asian Journal of Andrology (2021) 23, 249–258
www.asiaandro.com; www.ajandrology.com

Open Access

ORIGINAL ARTICLE

Sexual Function

The near-infrared dye IR-61 restores erectile function in a streptozotocin-induced diabetes model via mitochondrial protection

Xiao-Feng Yue[1], Chong-Xing Shen[1], Jian-Wu Wang[1], Lin-Yong Dai[1], Qiang Fang[1], Lei Long[2], Yi Zhi[1], Xue-Ru Li[3], Ya-Wei Wang[2], Gu-Fang Shen[2], Zu-Juan Liu[2], Chun-Meng Shi[2],Wei-Bing Li[1]

This study aimed to evaluate the therapeutic effect of IR-61, a novel mitochondrial heptamethine cyanine dye with antioxidant effects, on diabetes mellitus-induced erectile dysfunction (DMED). Eight-week-old male Sprague–Dawley rats were intraperitoneally injected with streptozotocin (STZ) to induce type 1 diabetes. Eight weeks after STZ injection, all rats were divided into three groups: the control group, DM group, and DM + IR-61 group. In the DM + IR-61 group, the rats were administered IR-61 (1.6 mg kg^{-1}) twice a week by intravenous injection. At week 13, erectile function was evaluated by determining the ratio of the maximal intracavernous pressure to mean arterial pressure, and the penises were then harvested for fluorescent imaging, transmission electron microscopy, histological examinations, and Western blot analysis. Whole-body imaging suggested that IR-61 was highly accumulated in the penis after intravenous injection. IR-61 treatment significantly improved the maximal ICP of diabetic rats. Additionally, IR-61 ameliorated diabetes-induced inflammation, apoptosis, and phenotypic transition of corpus cavernosum smooth muscle cells (CCSMCs) in penile tissue. IR-61 also attenuated mitochondrial damage, reduced reactive oxygen species production in the corpus cavernosum and upregulated sirtuin1 (SIRT1), sirtuin3 (SIRT3), nuclear factor (erythroid-derived 2)-like 2 (Nrf2), and heme oxygenase expression in penile tissue. In conclusion, IR-61 represents a potential therapeutic option for DMED by protecting the mitochondria of CCSMCs, which may be mediated by activation of the SIRT1, SIRT3, and Nrf2 pathways.

Asian Journal of Andrology (2021) **23**, 249–258; doi: 10.4103/aja.aja_69_20; published online: 01 January 2021

Keywords: corpus cavernosum smooth muscle cells; diabetes; erectile dysfunction; IR-61; mitochondria

INTRODUCTION

Erectile dysfunction (ED) is three times more common and occurs at a younger age in diabetic patients than in men without diabetes. Multiple etiological factors, including endothelial damage, smooth muscle dysfunction, neuropathy, inflammation, and cavernous fibrosis, are responsible for the pathogenesis of diabetes mellitus-induced erectile dysfunction (DMED).[1] Phosphodiesterase type 5 inhibitors (PDE5i), the first-line treatment for ED, show poor effects on DMED.[2] Glycemic control is also not sufficiently effective to improve erectile function in individuals with diabetes.[3] Although second-line therapy, such as intracavernous injection of stem cells or vasoactive drugs, has been suggested to be therapeutic in treating DMED, 41%–68% of patients dropped out of therapy early due to local complications, including penile pain, prolonged erections, priapism, and fibrosis.[4] Therefore, novel and convenient therapeutic methods are urgently needed.

The poor efficacy of PDE5i in treating DMED is associated with dysfunction in corpus cavernosum smooth muscle cells (CCSMCs), which play a central role in the course of erection.[5] Relaxation of CCSMCs increases arterial blood flow, elevates intracavernous pressure (ICP), and ultimately induces penile erection.[6] Phenotypic switching and apoptosis of CCSMCs impair the vasorelaxation mechanisms of the corpus cavernosum and participate in the pathogenesis of DMED. Similar to other smooth muscle cells (SMCs), CCSMCs can transform from a contractile phenotype to a synthetic phenotype in the early period of DMED, resulting in decreased expression of contractility-associated proteins such as calponin, smooth muscle 22α (SM22α), and α-smooth muscle actin (α-SMA), as well as overexpression of synthetic markers such as osteopontin (OPN) and vimentin.[7,8] Additionally, apoptosis of CCSMCs has been shown to be involved in DMED, and the suppression of apoptosis could improve erectile function in diabetic rats.[9]

Studies have suggested that mitochondrial damage in CCSMCs and endothelial cells contributes to the pathogenesis of organic ED.[10,11] Mitochondria are abundant in SMCs and are required for maintaining myogenic contraction of SMCs.[12] Mitochondrial dysfunction caused by diabetes impairs mitochondrial homeostasis and induces excessive reactive oxygen species (ROS) production, which triggers SMC phenotypic transformation and cell apoptosis.[13,14] In addition, chronic inflammation is another important pathogenetic factor associated with DMED.[15,16] Research findings demonstrate the key importance of

[1]Department of Urology, The Third Affiliated Hospital of Chongqing Medical University (Gener Hospital), Chongqing 401120, China; [2]Institute of Rocket Force Medicine, State Key Laboratory of Trauma, Burns and Combined Injury, Third Military Medical University, Chongqing 400038, China; [3]Department of Ophthalmology, The Third Affiliated Hospital of Chongqing Medical University (Gener Hospital), Chongqing 401120, China.
Correspondence: Dr. WB Li (liweibing63@cqmu.edu.cn) or Dr. CM Shi (shicm@tmmu.edu.cn)
Received: 22 December 2019; Accepted: 06 September 2020

mitochondria in innate immune signaling. Specifically, antimicrobial defense and sterile inflammation occur via nucleotide binding and oligomerization of domain-like receptor family pyrin domain-containing 3 (NLRP3) inflammasome activity.[17] In diabetes, NLRP3 can be activated by mitochondrial ROS overproduction and the release of mitochondrial DNA into the cytoplasm secondary to mitochondrial injury.[18] In addition to promoting inflammation, NLRP3 activation also promotes cell death and SMC phenotypic transformation.[19] These studies suggested that protecting mitochondria in penile tissues could be a useful treatment for DMED; however, this treatment has not been tested in a clinical setting. Therefore, the identification of a drug that can protect mitochondria and attenuate inflammation in the corpus cavernosum would greatly contribute to the clinical treatment of DMED.

IR-61 is a novel near-infrared (NIR) fluorescent heptamethine cyanine dye with preferential mitochondrial accumulation properties. A previous study indicated that IR-61 could improve mitochondrial function and increase antioxidant capacity by activating the nuclear factor (erythroid-derived 2)-like 2 (Nrf2) signaling pathway, thereby protecting mitochondria from oxidative injury.[20] Nrf2 is a major negative regulator of oxidative stress and promotes the transcription of many antioxidant enzymes, including heme oxygenase (HO-1). Activation of Nrf2 signaling has been shown to play a protective role in DMED.[21,22] Preliminary experiments suggested that rats selectively accumulated high concentrations of IR-61 in the penis after caudal vein injection. Considering these characteristics of IR-61, we hypothesized that the high accumulation of IR-61 in penile tissue may play a therapeutic role in DMED through mitochondrial protection and oxidation. In this study, we investigated the effects of IR-61 on erectile function and the pathological alterations in the corpus cavernosum in diabetic rats and explored the potential mechanisms.

MATERIALS AND METHODS

Chemicals, animals, and experimental design

The synthesis of IR-61 was performed according to a previously reported method.[20] Experiments were conducted on male Sprague–Dawley rats (8 weeks old, weighing 220 g–280 g) that were purchased from the animal facility of the Central Animal House Services of the Army Medical University (Third Military Medical University, Chongqing, China). The experiments and animal care procedures were approved by the Laboratory Animal Welfare and Ethics Committee of the AMU (Chongqing, SCXK 2012-0011, 01082012, China).

Streptozotocin (STZ; 60 mg kg^{-1}; dissolved in citrate buffer, pH = 4.0; Sigma-Aldrich, S0130, St. Louis, MO, USA) was administered by intraperitoneal injection. Only animals with two consecutive random blood glucose levels of >16.7 mmol l^{-1} were included in the study.[23] Eight weeks after the induction of diabetes, the rats were assigned to groups: normal control rats (control, n = 10), diabetic rats that were treated with vehicle (DM; n = 16), and diabetic rats that were treated with IR-61 (DM + IR-61; n = 21). Solid IR-61 was dissolved in dimethylsulfoxide (DMSO) at a concentration of 10 mmol l^{-1} and stored at −20°C. IR-61 was diluted 40 times with phosphate buffer saline (PBS) for injection. Intravenous injections of IR-61 (1.6 mg kg^{-1}) were performed twice a week. Blood glucose and body weight were measured every 2 weeks. The penile tissue was divided for the different analyses. Cavernous tissue of the size of a grain of rice was cut from the root of the penis and fixed with 2.5% glutaraldehyde (Aladdin, G105906, Shanghai, China) for electron microscopy. Half of the distal penile tissue was cryopreserved for Western blot. The remaining part was cut into two pieces, and one part was fixed in 4% paraformaldehyde solution for immunostaining and Masson's trichrome staining, while the other was embedded in Tissue-Tek O.C.T. Compound (Sakura, 4583, Miami, FL, USA) for frozen sectioning and staining.

Optical properties of IR-61

IR-61 was dissolved in water, methanol, 10% fetal bovine serum (FBS) or PBS at 37°C at a concentration of 2 mmol l^{-1}. After sufficient mixing, the absorption spectra of each solution were determined by a full-wavelength enzymatic spectrometer, and the fluorescence emission spectra of each solution were determined by a fluorescence spectrophotometer (Thermo Fisher Scientific, Waltham, MA, USA). Excitation wavelength was 740 nm, excitation and emission slit width was 5 nm, and scanning was conducted from 750 nm to 900 nm.

NIR imaging of IR-61 in vivo and ex vivo

At 6 h, 1 day, 2 days, and 5 days after injection, normal rats that had been intravenously injected with IR-61 (1.6 mg kg^{-1}) were anesthetized and subjected to NIR whole-body fluorescent imaging to trace the biodistribution of IR-61 *in vivo* with an In-Vivo FX professional imaging system (Kodak, Rochester, NY, USA).[20] The animals were then sacrificed, and their hearts, livers, lungs, spleens, kidneys, bladders, and penises were harvested for *ex vivo* imaging. To determine the IR-61 distribution in the corpus cavernosum, penile tissues were frozen and cut into slices (8 μm). Smooth muscle was then immunostained with goat anti-α-SMA (1:200; Abcam, ab21027, Cambridge, UK). The fluorescence signals of IR-61 and α-SMA were assessed using LAS AF Lite software (Leica, Weztlar, Germany).

Subcellular localization of IR-61 in CCSMCs

CCSMCs were isolated from Sprague-Dawley (SD) rats and cultured adherently.[24] Cells at passage 2 were harvested for fluorescence staining. Identification of CCSMCs was performed by immunofluorescence staining with goat anti-α-SMA (1:100; Abcam, ab21027) and rabbit anti-Desmin antibodies (1:100; Abcam, ab32362) as previously described.[25] To confirm the subcellular localization of IR-61, cultured CCSMCs were seeded in a 35 mm Petri dish and incubated with 10 mmol l^{-1} IR-61 for 20 min and 100 nmol l^{-1} MitoTracker Green (Invitrogen, M7514, Carlsbad, CA, USA) or 100 nmol l^{-1} LysoTracker Green (Invitrogen, L7526) for 30 min. Then, the cells were stained with Hoechst 33342 (Beyotime, C1025, Shanghai, China) and photographed by a fluorescence microscope (BX51, Olympus, Tokyo, Japan).

Erectile function measurement

Erectile function was assessed at 13 weeks after STZ induction. ICP and mean arterial pressure (MAP) were measured with the BL-420F multichannel signal collection processing system (Chengdu Implement Company, Chengdu, China) to evaluate erectile function as previously described.[26] The cavernous nerve (CN) stimulation parameters were 5 V at a frequency of 15 Hz with a pulse width of 1.2 ms for 1 min.

Histology, immunohistochemistry, and immunofluorescence

For the histological analysis, the corpus cavernosum tissue was fixed in 4% paraformaldehyde, embedded and sliced in a routine manner. Masson's trichrome, terminal deoxynucleotidyl transferase-mediated nick end labeling (TUNEL), and immunohistochemical and immunofluorescent staining were performed according to the literature.[3] The TUNEL assay was performed using an *in situ* cell death detection kit with fluorescein (Roche, 11684817910, Indianapolis, IN, USA). TUNEL was costained with goat anti-α-SMA (1:200; ab21027, Abcam) to evaluate the apoptotic levels of CCSMCs. For immunohistochemical

and immunofluorescence staining, the primary antibodies were rabbit anti-Desmin (1:200; Abcam, ab32362), goat anti-α-SMA (1:200; Abcam, ab21027), mouse anti-Calponin (1:200; Proteintech, 13938-1-AP, Rosemont, IL, USA), mouse anti-SM22α (1:100; Proteintech, 60213-1-Ig), rabbit anti-OPN (1:200; Abcam, ab8448), rabbit anti-Ras homolog gene family, member A (RhoA; 1:100; Proteintech, 10749-1-AP), rabbit anti-Rho-associated, coiled-coil containing protein kinase 1 (ROCK1; 1:100; Proteintech, 21850-1-AP), mouse anti-vimentin (1:200; Abcam, ab20346), rabbit anti-cleaved-caspase-3 (1:100; Abcam, ab13847), rabbit anti-sirtuin1 (SIRT1; 1:200; Proteintech, 13161-1-AP), rabbit anti-sirtuin3 (SIRT3; 1:200; Proteintech, 10099-1-AP), goat anti-NLRP3 (1:200; Abcam, ab4207), rabbit anti-caspase-1 (1:100; Abcam, ab179515), and mouse anti-apoptosis-associated speck-like protein containing a caspase-recruitment domain (ASC; 1:100; Santa Cruz Biotechnology, sc-514414, Santa Cruz, CA, USA). The sections were photographed and then quantitatively analyzed using ImageJ software (National Institutes of Health, Bethesda, MD, USA).

In situ detection of mitochondria and superoxide levels

To detect the mitochondrial mass of CCSMCs *in situ*, fresh frozen sections of corpus cavernosum tissues from all groups were incubated with MitoTracker Red (200 μmol l^{-1}; Invitrogen, M7512), fixed with 4% paraformaldehyde, and costained with Alexa Fluor 488-conjugated goat anti α-SMA. The mitochondrial mass of CCSMCs was imaged and assessed by confocal fluorescence microscopy (TCS SP5, Leica). Fresh frozen sections of penile tissues were incubated with MitoTracker Green (200 μmol l^{-1}; Invitrogen, M7514), Dihydroethidium (DHE; 10 μmol l^{-1}; Beyotime, S0063), and MitoSOX (10 μmol l^{-1}; Invitrogen, M36008) at 37°C in the dark for 20 min to measure mitochondrial content and *in situ* cytosolic and mitochondrial superoxide in the corpus cavernosum, respectively. Quantitative analysis of the fluorescence intensity was performed using ImageJ software.

Western blot analysis

The corpus cavernosum tissues were obtained from the penes after the penile skin, tunica albuginea, blood vessel, and urethra cavernosum were removed. Then, the cavernous tissues were lysed with Radio Immunoprecipitation Assay (RIPA) buffer (Beyotime, P0013) containing a protease inhibitor cocktail (Roche, 4693132001). Total protein was extracted, and the concentration was quantified using a BCA protein assay kit. Proteins with different molecular weights were separated by sodium dodecyl sulfate polyacrylamide gel electrophoresis (SDS-PAGE). The primary antibodies used were rabbit anti-Calponin (1:1000; Proteintech, 24855-1-AP), mouse anti-SM22α (1:1000; Proteintech, 60213-1-Ig), rabbit anti-OPN (1:1000; Abcam, ab8448), rabbit anti-SIRT1 (1:1000; Proteintech, 13161-1-AP), rabbit anti-SIRT3 (1:1000; Proteintech, 10099-1-AP), rabbit anti-NLRP3 (1:1000; Abcam, ab214185), rabbit anti-caspase-1 (1:1000; Proteintech, 22915-1-AP), rabbit anti-interleukin-1β (IL-1β; 1:1000; Abcam, ab9722), mouse anti-ASC (1:1000; Santa Cruz, sc-514414), rabbit anti-cleaved-caspase-3 (1:1000; Abcam, ab13847), rabbit anti-Nrf2 (1:1000; Proteintech, 66504-1-Ig), rabbit anti-HO-1 (1:1000; Abcam, ab13248), mouse anti-glyceraldehyde-3-phosphate dehydrogenase (GAPDH; 1:5000; Proteintech, 60004-1-Ig), and mouse anti-β-actin (1:5000; Proteintech, 60008-1-Ig). After incubation with horseradish peroxidase (HRP)-conjugated secondary antibodies, the polyvinylidene fluoride (PVDF) membrane was measured by a ChemiDoc XRS System (Bio-Rad, Hercules, CA, USA). The Western blot results were analyzed and quantified by ImageJ software.

Transmission electron microscopy (TEM)

The corpus cavernosum tissues were harvested, fixed in 4% glutaraldehyde overnight, fixed in 1% osmium tetroxide, dehydrated in graded ethanol, and embedded in fresh 100% resin. Ultrathin sections were cut and stained with 5% uranyl acetate and lead citrate and viewed by a fully trained expert in TEM (JEM-1400PLUS, JEOL, Tokyo, Japan) at 100 kV.

Statistical analyses

The data were expressed as the mean ± standard derivation (s.d.). Statistical analysis of experimental data was performed using GraphPad Prism 8.0 (GraphPad Software, La Jolla, CA, USA). One-way analysis of variance (ANOVA) or two-way ANOVA followed by Bonferroni *post hoc* test was used for comparisons. A Kruskal–Wallis test followed by Dunn's multiple comparison was used to analyze data with a skewed distribution. $P < 0.05$ was considered statistically significant.

RESULTS

Optical properties and subcellular localization of IR-61

The chemical structure of IR-61 is shown in **Supplementary Figure 1a**. The peaks of the absorption and emission spectra of IR-61 in methanol, 10% FBS, H_2O, and PBS were all in the NIR band (780 nm–850 nm). The spectral analysis confirmed the NIR fluorescence of IR-61 (**Supplementary Figure 1b** and **1c**). To determine the subcellular location of IR-61, we isolated and cultured primary CCSMCs from 8-week-old Sprague–Dawley rats. Cells were identified by immunofluorescent staining with α-SMA and Desmin, two specific antigens of SMCs (**Supplementary Figure 2**). Targeted accumulation of IR-61 in the mitochondria of CCSMCs was confirmed by colocalization with MitoTracker Green but not LysoTracker Green or Hoechst (**Supplementary Figure 1d**). These results support the claims that IR-61 is a mitochondria-targeting NIR dye, which is consistent with a previous study.

Biodistribution and accumulation of IR-61

According to the whole-body imaging results, rats administered IR-61 had a higher NIR fluorescence signal in the penis *in vivo* than rats treated with vehicle (**Figure 1a**). The detection of the intense fluorescence signal in the penis *in vivo* suggests that IR-61 could be used in the diagnosis and treatment of penile disease. The rats were sacrificed, and their vital organs were harvested for *ex vivo* imaging. We observed obviously stronger NIR fluorescence within the penis and bladder than in other organs. These results illustrate that IR-61 could accumulates in the penis and bladder, as proven by the NIR fluorescence intensities in the penis and bladder, which were significantly higher than those in other organs at 1 day, 2 days, and 5 days postintravenous administration ($P < 0.05$ for each; **Figure 1b**).

To determine the distribution of IR-61 in penile tissue, the corpus cavernosum tissues were frozen and sliced at 1 day and 5 days after injection for histological examination. Fluorescence microscopy revealed that IR-61 colocalized with α-SMA, a smooth muscle cell marker, suggesting the uptake of IR-61 by CCSMCs in the corpus cavernosum (**Figure 1c**) and thereby verifying the role of IR-61 in CCSMCs as the focus in this study.

Measurement of glycemia and body weight

As shown in **Figure 2a** and **2b**, there was no significant difference in blood glucose among the three groups at the beginning of the experiment (5.13 ± 0.72 mmol l^{-1}, 5.06 ± 0.74 mmol l^{-1}, and 5.07 ± 0.88 mmol l^{-1}). At the end of the study, the blood glucose

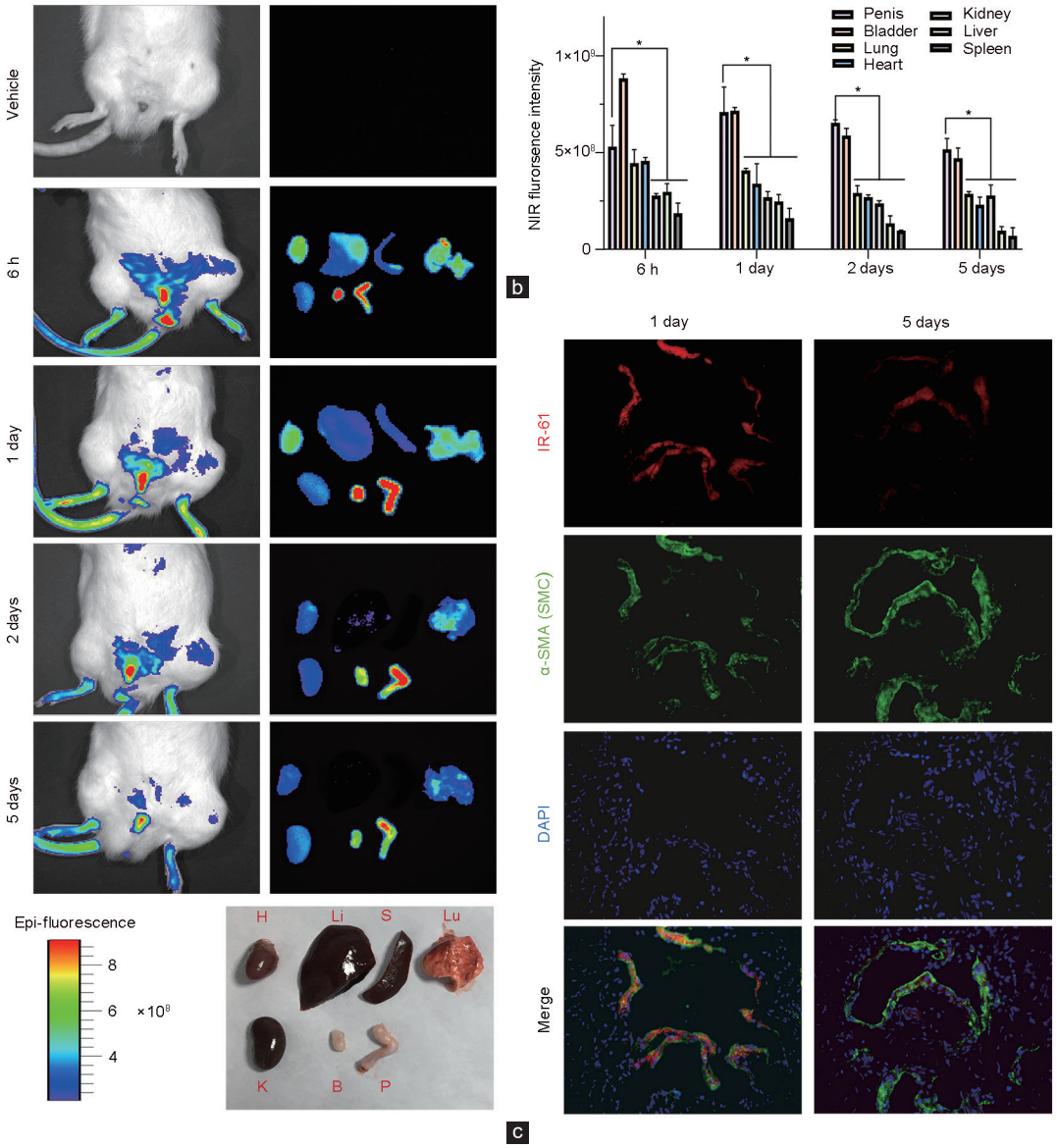

Figure 1: Biodistribution of IR-61 after intravenous administration. (**a**) *In vivo* and *ex vivo* NIR imaging of rats and their vital organs at 6 h, 1 day, 2 days, and 5 days after intravenous injection of IR-61. (**b**) Quantitative analysis of the NIR fluorescence intensities of vital organs at the indicated time points ($n = 4$ per group). $^*P < 0.05$, the NIR fluorescence intensities of indicated organs compared with that of the penis. (**c**) Fluorescence imaging of IR-61 (red) in corpus cavernosum tissues costained with α-SMA (green). Scale bar = 20 μm. NIR: near infrared; SMC: smooth muscle cell; α-SMA: α-smooth muscle actin; H: heart; Li: liver; S: spleen; Lu: lung; K: kidney; B: bladder; P: penis.

levels in the DM and DM + IR-61 groups (31.31 ± 2.63 mmol l^{-1} and 31.85 ± 2.09 mmol l^{-1}, respectively) were significantly higher than that in the control group (6.84 ± 1.09 mmol l^{-1}; $P < 0.0001$ for each). The blood glucose levels in the two diabetic groups showed no significant differences ($P > 0.99$). The initial body weight in each group showed no significant difference (250.70 ± 18.90 g, 239.81 ± 19.34 g, and 247.52 ± 17.90 g). The final body weight of the normal control group (552.90 ± 20.61 g) was much higher than that in the two diabetic groups (326.00 ± 40.85 g and 298.5 ± 57.67 g; $P < 0.0001$ for each). There was no significant difference in body weight between the DM and DM + IR-61 groups ($P > 0.99$). These results indicated that IR-61 did not change glycometabolism or body weight in STZ-induced diabetes mellitus.

IR-61 improved erectile function in diabetes

Erectile function was analyzed by the ratio of max ICP to MAP (ICP/MAP). The ICP/MAP ratios were significantly decreased in diabetic rats compared with normal rats ($P < 0.0001$). Notably, the ICP/MAP ratio in the DM + IR-61 group was higher than that in the DM group ($P < 0.0001$; **Figure 2c** and **2d**). These results demonstrated that the administration of IR-61 could improve the capacity for erection in diabetic rats.

IR-61 maintained CCSMCs in diabetes

Changes in morphology and the ratio of smooth muscle to collagen were observed using Masson's trichrome staining (**Supplementary Figure 3a**). The smooth muscle-to-collagen ratio

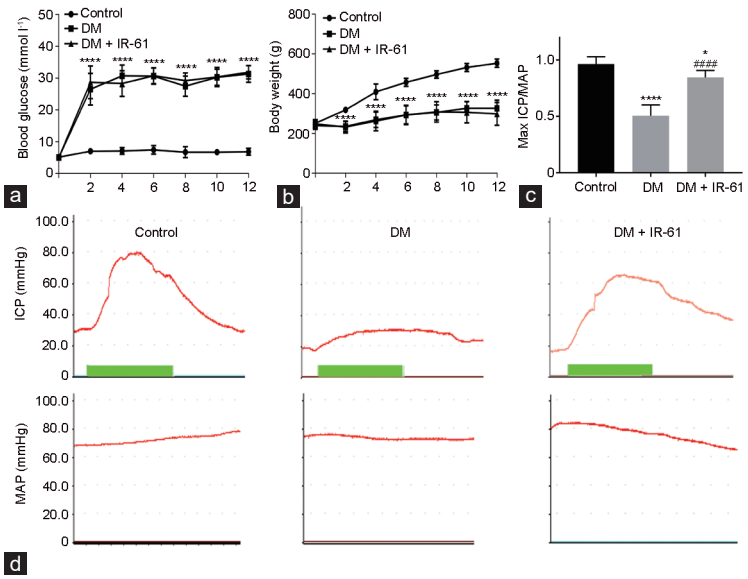

Figure 2: IR-61 improved erectile function in diabetic rats independent of blood glucose control. (**a**) Blood glucose and (**b**) body weight in each group after STZ injection ($n = 10$, 18 and 21 for each group). (**c**) Representative images of ICP and MAP for the control, DM, and DM + IR-61 groups at 5 V; green scale bars indicate 60 s electric stimulation. (**d**) Statistical analysis of the maximal ICP/MAP ratios in the three group ($n = 6$ per group). $^{*}P < 0.05$, the indicated group compared with the control group; $^{****}P < 0.0001$, the indicated group compared with the control group; $^{\#\#\#\#}P < 0.0001$, the indicated group compared with the DM group. STZ: streptozotocin; ICP: intracavernosal pressure; MAP: mean arterial pressure; DM: diabetes mellitus.

in the DM group was significantly reduced compared with that in the control group ($P < 0.001$). IR-61 treatment significantly reversed the reduction in the smooth muscle-to-collagen ratio ($P < 0.01$; **Supplementary Figure 3b**). Immunohistochemistry staining for Desmin to assess the smooth muscle content further confirmed that IR-61 partially restored the smooth muscle content in diabetic rats ($P < 0.01$; **Supplementary Figure 3c** and **3d**).

To examine the phenotypic switching of CCSMCs *in vivo*, the expression of contractile markers (α-SMA, Calponin, and SM22α) and synthetic markers (OPN and vimentin) in the corpus cavernosum was measured by Western blot and immunofluorescence. The Western blot results showed that OPN was more highly expressed in the DM group than in the other two groups ($P < 0.01$ for each). The protein levels of Calponin and SM22α were decreased in diabetic rats ($P < 0.001$ and $P < 0.0001$, respectively), and Calponin levels were rescued by IR-61 treatment ($P < 0.05$; **Figure 3b** and **3c**). Immunofluorescent staining showed that IR-61 increased the levels of SM22α and α-SMA ($P < 0.001$ for both) while lowering the expression of OPN and vimentin in diabetic rats ($P < 0.05$ and $P < 0.001$, respectively; **Figure 3a**, **3d,** and **3e**; **Supplementary Figure 4a**, **4c,** and **4d**). As shown in **Supplementary Figure 4b**, **4e** and **4f**, Rho A and ROCK1, which are critical for the translation of contractile proteins in SMCs, showed significantly lower fluorescence intensities in the DM group than those in the control group ($P < 0.01$ and $P < 0.001$, respectively). IR-61 administration increased Rho A and ROCK1 levels in diabetic rats ($P < 0.05$ and $P < 0.01$, respectively). These data suggest that IR-61 can maintain the contractile phenotype of CCSMCs in diabetes.

Dual staining of TUNEL and α-SMA in cavernous tissue demonstrated a significant increase in the number of apoptotic cells among CCSMCs in the DM group compared to that of the control and DM + IR-61 groups ($P < 0.001$ for each, **Figure 4a** and **4b**). Western blot analysis showed higher protein levels of cleaved-caspase-3 in diabetic rats than in normal rats, which was ameliorated by IR-61 ($P < 0.001$ for each; **Figure 4e** and **4f**). Immunofluorescence staining of cleaved-caspase-3 showed similar results (**Figure 4c** and **4d**). These data indicate the anti-apoptotic effect of IR-61 in cavernous tissue and CCSMCs in diabetes.

IR-61 suppressed diabetes-induced inflammation in the corpus cavernosum

The protein levels of NLRP3 and its downstream molecules, such as pro-caspase-1, caspase-1 p20, ASC, and IL-1β, were analyzed using immunofluorescence staining and Western blot. The fluorescence intensities of NLRP3, ASC, and caspase-1 were increased in the corpus cavernosum in the DM group. However, these observed increases were mitigated by IR-61 (**Supplementary Figure 5a–5c** and **6**). Similarly, the Western blot results revealed that IR-61 treatment attenuated the upregulation of NLRP3, pro-caspase-1, caspase-1 p20, IL-1β, and ASC in the cavernous tissues of diabetic rats ($P < 0.01$, $P < 0.05$, $P < 0.001$, $P < 0.001$, and $P < 0.01$, respectively; **Supplementary Figure 5d** and **5e**). These data indicated that IR-61 was able to reduce diabetes-induced inflammatory cell infiltration and NLRP3 inflammasome activation, thereby suppressing inflammation in the corpus cavernosum.

IR-61 mitigated mitochondrial damage and mitochondrial ROS production

To determine the number of active mitochondria in CCSMCs, frozen sections were co-stained with MitoTracker Red and α-SMA (**Figure 5a**), and the results showed that MitoTracker Red was mainly localized in smooth muscle areas. The fluorescence intensity of MitoTracker Red was reduced in diabetic rats ($P < 0.01$) and was rescued by IR-61 administration ($P < 0.01$), indicating that IR-61 could restore the mitochondrial mass in CCSMCs in diabetes (**Figure 5e**). Fluorescence staining with MitoTracker Green verified that IR-61 rescued the mitochondrial capacity in the cavernous tissue of diabetic rats ($P < 0.05$; **Supplementary Figure 7**). The ultrastructures of CCSMCs were observed by TEM, which revealed that CCSMCs

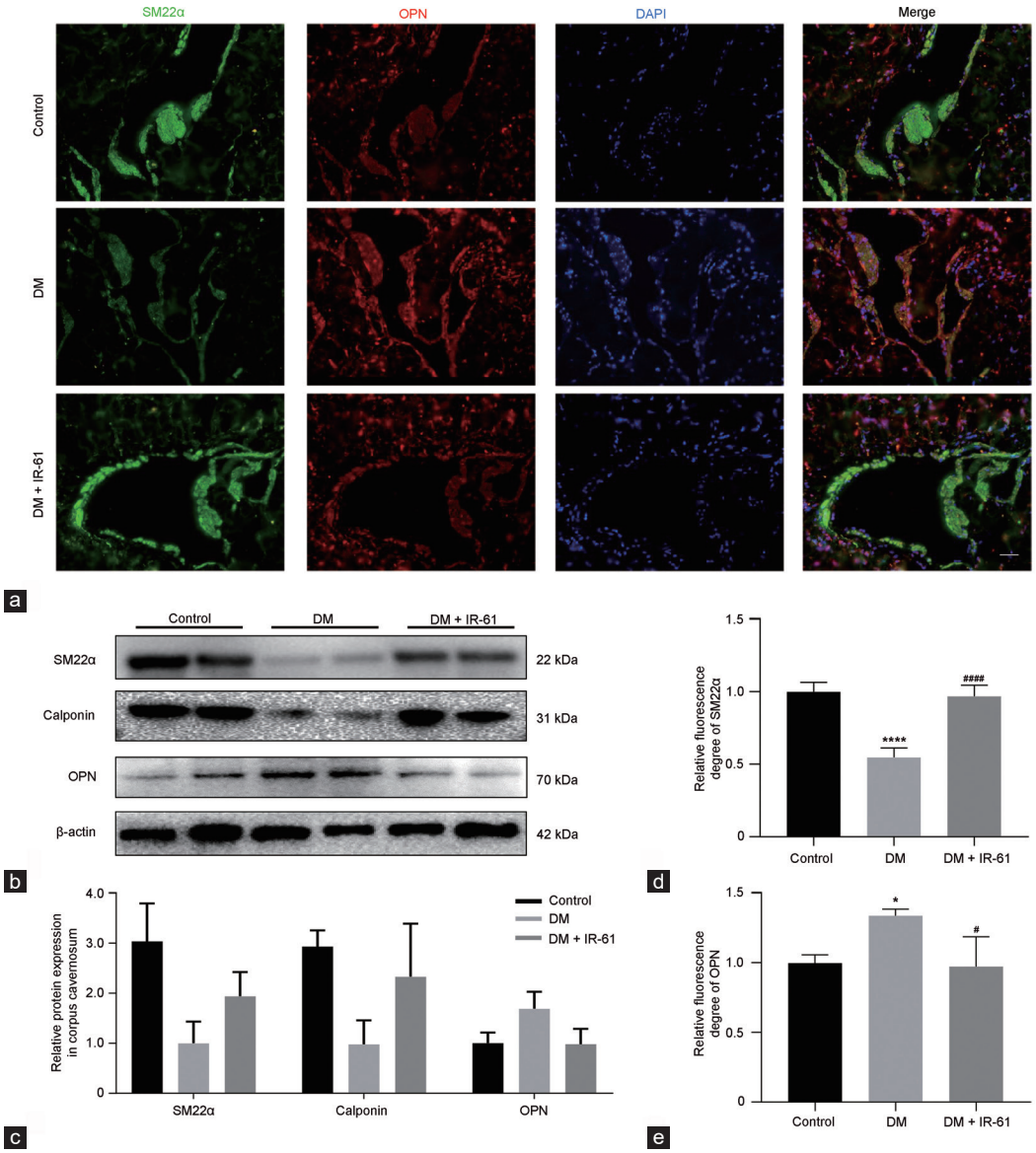

Figure 3: IR-61 mitigated the phenotypic transition of CCSMCs in STZ-induced diabetic rats. (**a**) Dual staining for SM22α and OPN in the penile corpus cavernosum ($n = 4$ per group). Scale bar=20 μm. (**b**) Protein levels of SM22α, calponin, and OPN in the corpus cavernosum of each group were measured by Western blot ($n = 4$ per group). (**c**) Quantitative analysis of protein levels of SM22α, calponin, and OPN in the corpus cavernosum. Quantitative analysis of fluorescence intensity of (**d**) SM22α and (**e**) OPN. $^{*}P < 0.05$, the indicated group compared with the Control group; $^{****}P < 0.0001$, the indicated group compared with the Control group; $^{\#\#\#\#}P < 0.0001$, the indicated group compared with the DM group. CCSMCs: corpus cavernosum smooth muscle cells; STZ: streptozotocin; SM22α: smooth muscle 22α; OPN: osteopontin; DM: diabetes mellitus; DAPI: 4',6-diamidino-2-phenylindole.

in STZ-induced diabetic rats exhibited increased mitochondrial vacuolization, and IR-61 attenuated mitochondrial damage in CCSMCs in diabetic rats (**Figure 5b**). Frozen sections of the corpus cavernosum stained with DHE and MitoSOX (**Figure 5c** and **5d**) were used to measure mitochondrial and cellular superoxide levels. Fluorescence intensity analysis of DHE and MitoSOX showed that both cellular and mitochondrial superoxide levels were elevated in the DM group ($P < 0.01$ for each) and were blocked by IR-61 treatment ($P < 0.05$ and $P < 0.01$, respectively), which demonstrated the antioxidant effect of IR-61 (**Figure 5e** and **5f**).

The localization of SIRT1 and SIRT3 was determined by immunofluorescent staining with α-SMA (**Figure 6a** and **6b**). SIRT1 and SIRT3 were colocalized with α-SMA, which confirmed that SIRT1 and SIRT3 were mainly expressed in the cytoplasm of CCSMCs in penile tissue. Fluorescence intensity analysis suggested that IR-61 could increase the expression of SIRT1 in diabetic cavernous tissue ($P < 0.001$; **Figure 6d**).

Western blot indicated that the protein levels of SIRT1 and SIRT3 significantly declined in the diabetic rats ($P < 0.01$ and $P < 0.0001$, respectively) and were restored by the administration of IR-61 ($P < 0.05$ and $P < 0.001$, respectively; **Figure 6c** and **6e**). The protein levels of Nrf2 and HO-1 were upregulated in the DM group ($P < 0.01$ for each) and were further elevated by IR-61 administration ($P < 0.001$ and $P < 0.05$, respectively; **Figure 6f** and **6g**). These findings suggested that IR-61 could potentially increase penile levels of SIRT1, SIRT3, Nrf2 and HO-1 in diabetic rats, which may be related to the cytoprotective effect of IR-61 on CCSMCs.

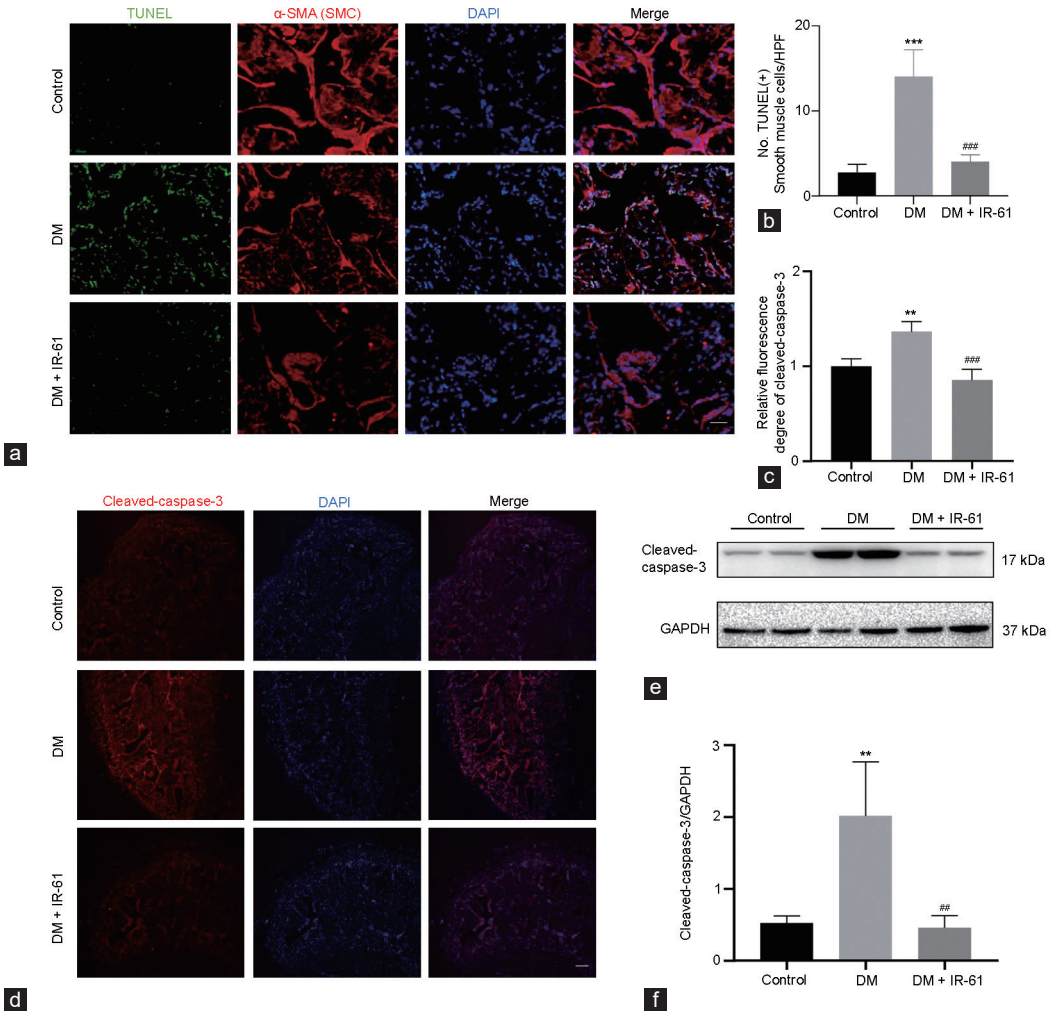

Figure 4: IR-61 reduced CCSMC apoptosis in diabetic rats. (**a**) Representative images of dual staining of the penile corpus cavernosum with TUNEL (green) and α-SMA (red); scale bar =20 μm. (**b**) Number of apoptotic CCSMCs per high-power field ($n = 4$ per group). (**c**) The levels of cleaved-caspase-3 in penile tissue were measured by immunostaining ($n = 4$ per group). (**d**) Representative images of immunostaining of cleaved-caspase-3 in the cavernous tissue. Scale bar=100 μm. (**e**) Western blot analysis of cleaved-caspase-3 in the corpus cavernosum. (**f**) Quantitative analysis of Western blot results of SM22α, calponin, and OPN ($n = 4$ per group). $^{**}P < 0.005$, the indicated group compared with the control group; $^{***}P < 0.001$, the indicated group compared with the control group; $^{\#\#}P < 0.01$, the indicated group compared with the DM group; $^{\#\#\#}P < 0.001$, the indicated group compared with the DM group. CCSMCs: corpus cavernosum smooth muscle cells; SMC: smooth muscle cell; TUNEL: terminal deoxynucleotidyl transferase-mediated nick end labeling; HPF: high power filed; α-SMA: α-smooth muscle actin; SM22α: smooth muscle 22α; DM: diabetes mellitus; DAPI: 4',6-diamidino-2-phenylindole; GAPDH: glyceraldehyde-3-phosphate dehydrogenase.

DISCUSSION

Although the treatment of erectile dysfunction has been well studied, treatment for DMED remains a challenge. Patients with DMED show limited responsiveness to PDE5i, the first-line therapy for ED. Intracavernous injections, the second-line therapy, have been demonstrated to be an efficient treatment method, but the administration is psychologically difficult for patients to accept and can lead to complications such penile pain, prolonged erections, priapism, and fibrosis, which limit their clinical efficacy.[4] Hence, a convenient and safe strategy is needed for treating DMED. IR-61 is an NIR heptamethine fluorescent dye with cytoprotective effects and antioxidative properties that exclusively accumulates in the mitochondria and exhibits mitoprotective and antioxidant effects by activating the Nrf2 pathway.[20] The activation of Nrf2 signaling has been shown to play a protective role on DMED.[21,22] Herein, we first determined that intravenously administered IR-61 was able to accumulate in penile tissue and restore erectile function in STZ-induced diabetic rats, which indicated that IR-61 may be a potential candidate for the treatment of DMED.

Histological examination showed that IR-61 was mainly taken up by CCSMCs in the corpus cavernosum. CCSMCs provide structural support for vasodilation, control blood flow into the cavernous sinus, and play a vital role during penile erection.[6] Dysfunction in CCSMCs is one of the principal causes of DMED. Some research reported that diabetes induced excessive contraction of CCSMCs by activating the RhoA/ROCK pathway, which could directly trigger SMC contraction through Ca^{2+}-independent regulation and increase the expression of contractile makers (Myocardin, SM22α, Calponin, and α-SMA), eventually leading to DMED.[27–29] However, other studies suggested that induced CCSMC apoptosis and phenotypic transformation,

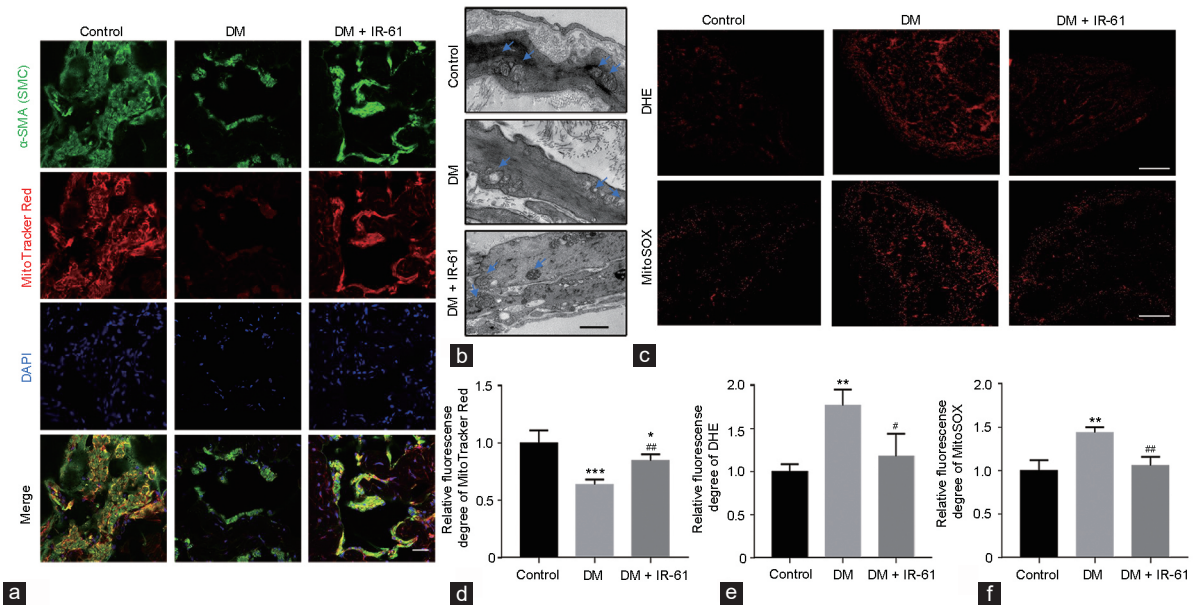

Figure 5: IR-61 alleviated mitochondrial damage caused by diabetes. (**a**) Mitochondrial mass in CCSMCs was measured by MitoTracker Red and α-SMA costaining of frozen sections of penile tissue (n = 4 per group). Scale bar = 20 μm. (**b**) Representative transmission electron micrographs showing the morphology and structure of mitochondria in CCSMCs. The arrows indicate mitochondria; scale bar = 0.5 μm. (**c**) Representative DHE staining and MitoSOX staining in each group; scale bar = 100 μm (n = 3 per group). Quantitative analysis of fluorescence intensity of (**d**) DHE, (**e**) MitoSOX, and (**f**) MitoTracker Red. $^{**}P < 0.01$, the indicated group compared with the control group; $^{\#}P < 0.05$, the indicated group compared with the DM group; $^{\#\#}P < 0.01$, the indicated group compared with the DM group. SMC: smooth muscle cell; DHE: dihydroethidium; CCSMCs: corpus cavernosum smooth muscle cells; α-SMA: α-smooth muscle actin; DM: diabetes mellitus; DAPI: 4',6-diamidino-2-phenylindole.

which impair the contractile and relaxation functions of CCSMCs, were involved in the pathogenesis of DMED.[8,30] In our study, CCSMC apoptosis and phenotypic transition in diabetic rats were confirmed. Additionally, the levels of Rho A and ROCK1 were significantly lower in the DM group than in the other groups. To our knowledge, this is the first report showing that the downregulation of the Rho A/ROCK pathway was also associated with DMED. These findings indicate that the loss of CCSMC contractility contributes to erectile function impairment in this diabetic rat model. IR-61 significantly alleviated the phenotypic transition and apoptosis of CCSMCs in diabetes, thereby recovering the loss of smooth muscle content in the corpus cavernosum.

Herein, we found that the corpus cavernosum of diabetic rats had significantly increased protein levels of NLRP3, ASC, IL-1β, pro-caspase-1, and caspase-1 p20. Chronic inflammation is one of the major factors associated with diabetic cardiovascular diseases, including DMED.[15,31] IL-1β, a potent proinflammatory cytokine, can impair cavernosum endothelial cells and lead to ED.[32] The NLRP3 inflammasome, composed of the NLRP3 protein, the adaptor protein ASC, and the cysteine protease pro-caspase-1, is an important regulator of the innate immune response, and its activation plays a crucial role in the pathogenesis of diabetes and diabetic complications. Diabetes-related mitochondrial dysfunction has been considered to be pivotal in this process.[33–35] It has been documented that activating the NLRP3 inflammasome could boost caspase-1-dependent pyroptosis and caspase-3-dependent apoptosis via a mitochondrial pathway.[36] Furthermore, several studies have revealed that SMC phenotypic transformation is promoted by NLRP3 inflammasome activation in spontaneously hypertensive rats and Ang II-induced hypertensive mice.[19,37] However, IR-61 administration blocked these alterations, demonstrating its anti-inflammatory effects.

In this study, diabetes-induced mitochondrial injury in CCSMCs was confirmed by decreased mitochondrial mass, increased mitochondrial ROS production, and mitochondrial vacuolization, while mitochondrial damage was alleviated by IR-61 administration. It has been well established that maintaining mitochondrial homeostasis could retain the contractile phenotype and reduce the apoptosis of SMCs.[38] Additionally, excessive mitochondrial ROS production and the release of mitochondrial DNA into the cytoplasm secondary to mitochondrial damage are capable of activating the NLRP3 inflammasome.[39] Additionally, IR-61 increased the protein levels of SIRT1, SIRT3 and Nrf2 in diabetic rats. SIRT1 and SIRT3 are two well-characterized members of the sirtuin family that play important roles in regulating mitochondrial function and maintaining mitochondrial homeostasis.[18] Decreases in SIRT1 and SIRT3 have been considered to be involved in the pathogenesis of ED induced by diabetes and other cardiovascular diseases, and the activation of SIRT1 could reduce inflammation in cavernous tissue and maintain smooth muscle levels, thereby improving DMED.[40–42] The activation of Nrf2, which is also involved in the regulation of mitochondrial homeostasis in diabetes by modulating mitochondrial biogenesis and mitochondrial membrane potential, could improve erectile dysfunction in STZ-induced diabetic rats through the upregulation of HO-1.[21,43] Moreover, SIRT1 has been regarded as an upstream regulator of the Nrf2 signaling pathway. Activating Nrf2 signaling enhances the transcription of SIRT3 and HO-1, which play pivotal roles in the alleviation of oxidative injuries and inflammation.[44–46] The upregulation of SIRT1, SIRT3, Nrf2 and HO-1 in diabetic rats might be the mechanism by which IR-61 protects mitochondria from oxidative stress and improves DMED.

One major limitation of this study is that we failed to establish the cell model because high glucose conditions were not sufficient to

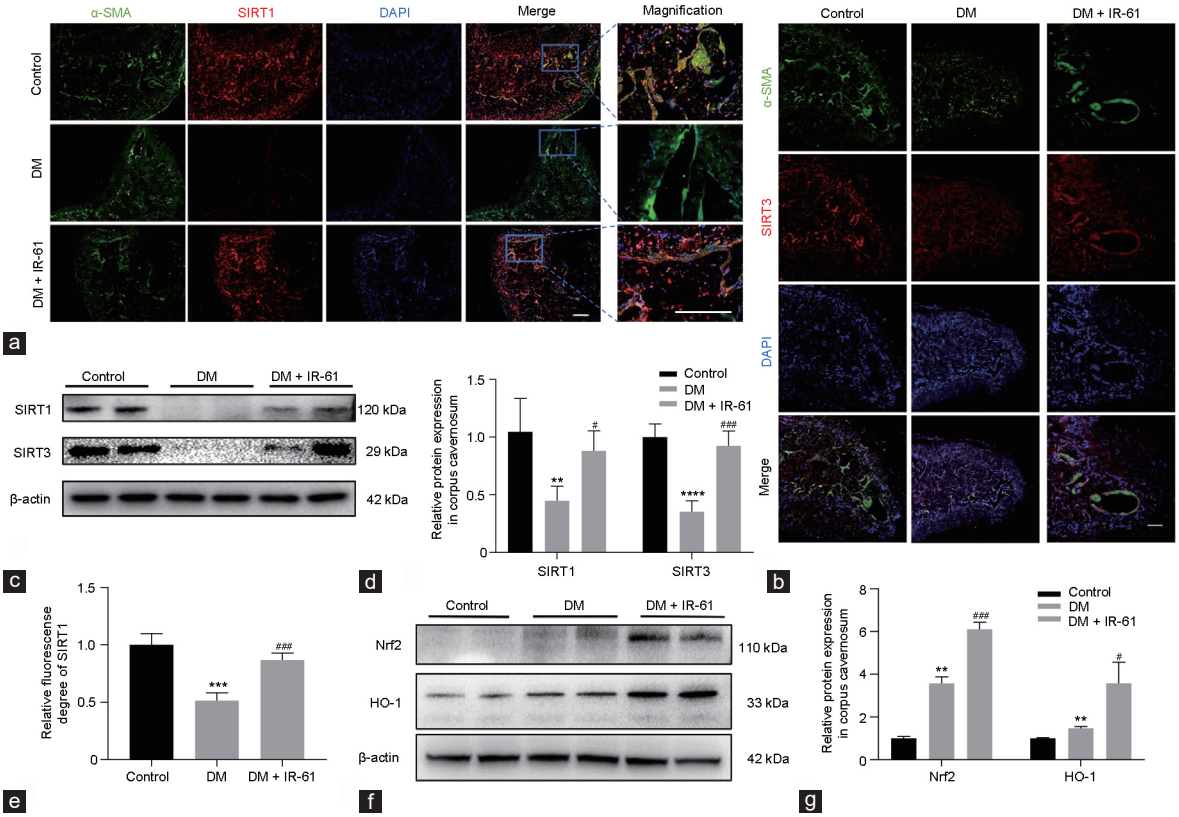

Figure 6: IR-61 increased Nrf2 activation and restored SIRT1 and SIRT3 expression in cavernous tissue. (**a**) Representative images of SIRT1 costaining with α-SMA. Scale bar = 100 μm. (**b**) Representative images of SIRT3 co-staining with α-SMA and quantitative analysis of the fluorescence intensity of SIRT3. Scale bar = 100 μm (n = 4 per group). (**c**) Representative images of Western blot analysis of SIRT1 and SIRT3. (**d**) Quantitative analysis of the SIRT1 fluorescence intensity (n = 4 per group). (**e**) Relative SIRT1 and SIRT3 protein levels in the cavernous tissue (n = 4–5 each group). (**f**) Western blot analysis of Nrf2 and HO-1 in the cavernous tissue. (**g**) Relative protein levels of Nrf2 and HO-1 in the corpus cavernosum (n = 4 per group). $^{*}P < 0.05$, the indicated group compared with the control group; $^{**}P < 0.01$, the indicated group compared with the control group; $^{***}P < 0.001$, the indicated group compared with the control group; $^{\#}P < 0.05$, the indicated group compared with the DM group; $^{\#\#}P < 0.01$, the indicated group compared with the DM group; $^{\#\#\#}P < 0.001$, the indicated group compared with the DM group. Nrf2: nuclear factor (erythroid-derived 2)-like 2; SIRT1: sirtuin1; SIRT3: sirtuin3; HO-1: heme oxygenase; α-SMA: α-smooth muscle actin; DM: diabetes mellitus; DAPI: 4',6-diamidino-2-phenylindole.

steadily induce phenotypic transition, apoptosis and inflammation in primary cultured CCSMCs. Therefore, we did not investigate and verify the protective mechanisms of IR-61 in cellular experiments. Another limitation is that our study was performed on a rat model of type 1 diabetes, while type 2 diabetes mellitus (T2DM) is the most common type of diabetes. The effect of IR-61 on T2DM and its complications should be further investigated.

CONCLUSION

In this study, we first reported that IR-61 improved erectile function, suppressed inflammation in the corpora cavernosa, and reduced CCSMC phenotype transition and apoptosis in the STZ-induced diabetic rat model. These effects might be related to mitoprotection mediated by the SIRT1, SIRT3, and Nrf2 signaling pathways (**Supplementary Figure 8**). These findings highlight the potential of IR-61 as a novel therapeutic candidate for treating DMED.

AUTHOR CONTRIBUTIONS

XFY and CXS conceptualized this study, carried out main studies and drafted the manuscript. JWW and LYD participated in the animal care and surgery. QF, YZ, and YWW revised the manuscript. XRL and GFS participated the histology. LL carried out the chemical synthesis. ZJL performed the statistical analysis. WBL and CMS supervised the whole work. All authors read and approved the final manuscript.

COMPETING INTERESTS

All authors declared no competing interests.

ACKNOWLEDGMENTS

This work was financially supported by the National Key Research and Development Program (2016YFC1000805), University Innovation Team Building Program of Chongqing (CXTDG201602020) and Science and Technology Research Program of Chongqing Municipal Education Commission (KJQN202000433).

Supplementary Information is linked to the online version of the paper on the *Asian Journal of Andrology* website.

REFERENCES

1 Yin GN, Choi MJ, Kim WJ, Kwon MH, Song KM, *et al.* Inhibition of Ninjurin 1 restores erectile function through dual angiogenic and neurotrophic effects in the diabetic mouse. *Proc Natl Aca Sci U S A* 2014; 111: E2731–40.

2 Penson DF, Latini DM, Lubeck DP, Wallace KL, Henning JM, *et al.* Do impotent men with diabetes have more severe erectile dysfunction and worse quality of life than the general population of impotent patients? Results from the Exploratory Comprehensive Evaluation of Erectile Dysfunction (ExCEED) database. *Diabetes Care* 2003; 26: 1093–9.

3 Wang L, Xu Y, Li H, Lei H, Guan R, *et al*. Antioxidant icariside II combined with insulin restores erectile function in streptozotocin-induced type 1 diabetic rats. *J Cell Mol Med* 2015; 19: 960–9.
4 Phé V, Rouprêt M. Erectile dysfunction and diabetes: a review of the current evidence-based medicine and a synthesis of the main available therapies. *Diabetes Metab* 2012; 38: 1–13.
5 Burchardt T, Burchardt M, Karden J, Buttyan R, Shabsigh A, *et al*. Reduction of endothelial and smooth muscle density in the corpora cavernosa of the streptozotocin induced diabetic rat. *J Urol* 2000; 164: 1807–11.
6 Christ GJ. The penis as a vascular organ. The importance of corporal smooth muscle tone in the control of erection. *Urol Cli North Am* 1995; 22: 727–45.
7 Frismantiene A, Philippova M, Erne P, Resink TJ. Smooth muscle cell-driven vascular diseases and molecular mechanisms of VSMC plasticity. *Cell Signal* 2018; 52: 48–64.
8 Li WJ, Xu M, Gu M, Zheng DC, Guo J, *et al*. Losartan Preserves Erectile function by suppression of apoptosis and fibrosis of corpus cavernosum and corporal veno-occlusive dysfunction in diabetic rats. *Cell Physiol Biochem* 2017; 42: 333–45.
9 Park K, Ryu KS, Li WJ, Kim SW, Paick JS. Chronic treatment with a type 5 phosphodiesterase inhibitor suppresses apoptosis of corporal smooth muscle by potentiating Akt signalling in a rat model of diabetic erectile dysfunction. *Eur Urol* 2008; 53: 1282–8.
10 Zhang MG, Wang XJ, Shen ZJ, Gao PJ. Long-term oral administration of 5α-reductase inhibitor attenuates erectile function by inhibiting autophagy and promoting apoptosis of smooth muscle cells in corpus cavernosum of aged rats. *Urology* 2013; 82: 743.e9–15.
11 Mostafa ME, Senbel AM, Mostafa T. Effect of chronic low-dose tadalafil on penile cavernous tissues in diabetic rats. *Urology* 2013; 81: 1253–9.
12 Park SY, Gifford JR, Andtbacka RH, Trinity JD, Hyngstrom JR, *et al*. Cardiac, skeletal, and smooth muscle mitochondrial respiration: are all mitochondria created equal? *Am J Physiol Heart Circ Physiol* 2014; 307: H346–52.
13 Yang M, Fang J, Liu Q, Wang Y, Zhang Z. Role of ROS-TRPM7-ERK1/2 axis in high concentration glucose-mediated proliferation and phenotype switching of rat aortic vascular smooth muscle cells. *Biochem Bioph Res Co* 2017; 494: 526–33.
14 Zhang Y, Xia G, Zhang Y, Liu J, Liu X, *et al*. Palmitate induces VSMC apoptosis via toll like receptor (TLR)4/ROS/p53 pathway. *Atherosclerosis* 2017; 263: 74–81.
15 Lu J, Xin Z, Zhang Q, Cui D, Xiao Y, *et al*. Beneficial effect of PEDF-transfected ADSCs on erectile dysfunction in a streptozotocin-diabetic rat model. *Cell Tissue Res* 2016; 366: 623–37.
16 Trebatický B, Žitňanová I, Dvořáková M, Országhová Z, Paduchová Z, *et al*. Role of oxidative stress, adiponectin and endoglin in the pathophysiology of erectile dysfunction in diabetic and non-diabetic men. *Physiol Res* 2019; 68: 623–31.
17 Sandhir R, Halder A, Sunkaria A. Mitochondria as a centrally positioned hub in the innate immune response. *Biochim Biophys Acta Mol Basis Dis* 2017; 1863: 1090–7.
18 Rovira-Llopis S, Apostolova N, Bañuls C, Muntané J, Rocha M, *et al*. Mitochondria, the NLRP3 inflammasome, and sirtuins in type 2 diabetes: new therapeutic targets. *Antioxid Redox Signal* 2018; 29: 749–91.
19 Sun HJ, Ren XS, Xiong XQ, Chen YZ, Zhao MX, *et al*. NLRP3 inflammasome activation contributes to VSMC phenotypic transformation and proliferation in hypertension. *Cell Death Dis* 2017; 8: e3074.
20 Wang X, Chen ZL, Luo SL, Jin TT, Wang Y, *et al*. Development of therapeutic small-molecule fluorophore for cell transplantation. *Adv Funct Mater* 2016; 26: 8397-407.
21 Hu LL, Zhang KQ, Tian T, Zhang H, Fu Q. Probucol improves erectile function via activation of Nrf2 and coordinates the HO-1/DDAH/PPAR-γ/eNOS pathways in streptozotocin-induced diabetic rats. *Biochem Bioph Res Co* 2018; 507: 9–14.
22 Alves-Lopes R, Neves KB, Montezano AC, Harvey A, Carneiro FS, *et al*. Internal pudental artery dysfunction in diabetes mellitus is mediated by NOX1-Derived ROS-, Nrf2-, and Rho kinase-dependent mechanisms. *Hypertension* 2016; 68: 1056–64.
23 Fan M, Xu X, He X, Chen L, Qian L, *et al*. Protective effects of hydrogen-rich saline against erectile dysfunction in a streptozotocin induced diabetic rat model. *J Urol* 2013; 190: 350–6.
24 Wei AY, He SH, Zhao JF, liu Y, Liu Y, *et al*. Characterization of corpus cavernosum smooth muscle cell phenotype in diabetic rats with erectile dysfunction. *Int J Impot Res* 2012; 24: 196–201.
25 Zhang HB, Wang ZQ, Chen FZ, Ding W, Liu WB, *et al*. Maintenance of the contractile phenotype in corpus cavernosum smooth muscle cells by Myocardin gene therapy ameliorates erectile dysfunction in bilateral cavernous nerve injury rats. *Andrology* 2017; 5: 798–806.
26 Chen Z, Han X, Ouyang X, Fang J, Huang X, *et al*. Transplantation of induced pluripotent stem cell-derived mesenchymal stem cells improved erectile dysfunction induced by cavernous nerve injury. *Theranostics* 2019; 9: 6354–68.
27 Zhang Y, Jia L, Zhang Y, Ji W, Li H. Angiotensin II silencing alleviates erectile dysfunction through down-regulating the Rhoa/Rho kinase signaling pathway in rats with diabetes mellitus. *Cell Physiol Biochem* 2018; 45: 419–27.
28 Sopko NA, Hannan JL, Bivalacqua TJ. Understanding and targeting the Rho kinase pathway in erectile dysfunction. *Nat Rev Urol* 2014; 11: 622–8.
29 Li J, Jiang J, Yin H, Wang L, Tian R, *et al*. Atorvastatin inhibits myocardin expression in vascular smooth muscle cells. *Hypertension* 2012; 60: 145–53.
30 He S, Zhang T, Liu Y, Liu L, Zhang H, *et al*. Myocardin restores erectile function in diabetic rats: phenotypic modulation of corpus cavernosum smooth muscle cells. *Andrologia* 2015; 47: 303–9.
31 Ferrucci L, Fabbri E. Inflammageing: chronic inflammation in ageing, cardiovascular disease, and frailty. *Nat Rev Cardiol* 2018; 15: 505–22.
32 Demirtaş Şahin T, Yazir Y, Utkan T, Gacar G, Halbutoğulları ZS, *et al*. Depression induced by chronic stress leads to penile cavernosal dysfunction: protective effect of anti-TNF-α treatment. *Can J Physiol Pharm* 2018; 96: 933–42.
33 Liu D, Zeng X, Li X, Mehta JL, Wang X. Role of NLRP3 inflammasome in the pathogenesis of cardiovascular diseases. *Basic Res Cardiol* 2018; 113: 5.
34 Liu Q, Zhang D, Hu D, Zhou X, Zhou Y. The role of mitochondria in NLRP3 inflammasome activation. *Mol Immunol* 2018; 103: 115–24.
35 Zeng C, Wang R, Tan H. Role of pyroptosis in cardiovascular diseases and its therapeutic implications. *Int J Biol Sci* 2019; 15: 1345–57.
36 Vince JE, De Nardo D, Gao W, Vince AJ, Hall C, *et al*. The mitochondrial apoptotic effectors BAX/BAK activate caspase-3 and -7 to trigger NLRP3 inflammasome and caspase-8 driven IL-1β activation. *Cell Rep* 2018; 25: 2339–53.e4.
37 Ren XS, Tong Y, Ling L, Chen D, Sun HJ, *et al*. NLRP3 gene deletion attenuates angiotensin II-Induced phenotypic transformation of vascular smooth muscle cells and vascular remodeling. *Cell Physiol Biochem* 2017; 44: 2269–80.
38 Nahapetyan H, Moulis M, Grousset E, Faccini J, Grazide MH, *et al*. Altered mitochondrial quality control in Atg7-deficient VSMCs promotes enhanced apoptosis and is linked to unstable atherosclerotic plaque phenotype. *Cell Death Dis* 2019; 10: 119.
39 Shimada K, Crother TR, Karlin J, Dagvadorj J, Chiba N, *et al*. Oxidized mitochondrial DNA activates the NLRP3 inflammasome during apoptosis. *Immunity* 2012; 36: 401–14.
40 Kataoka T, Hotta Y, Maeda Y, Kimura K. Assessment of androgen replacement therapy for erectile function in rats with type 2 diabetes mellitus by examining nitric oxide-related and inflammatory factors. *J Sex Med* 2014; 11: 920–9.
41 Yu W, Wan Z, Qiu XF, Chen Y, Dai YT. Resveratrol, an activator of SIRT1, restores erectile function in streptozotocin-induced diabetic rats. *Asian J Androl* 2013; 15: 646–51.
42 Freitas M, Rodrigues AR, Tomada N, Fonseca J, Magalhães A, *et al*. Effects of aging and cardiovascular disease risk factors on the expression of sirtuins in the human corpus cavernosum. *J Sex Med* 2015; 12: 2141–52.
43 Kowluru RA, Mishra M. Epigenetic regulation of redox signaling in diabetic retinopathy: role of Nrf2. *Free Radic Biol Med* 2017; 103: 155–64.
44 Zhao MW, Yang P, Zhao LL. Chlorpyrifos activates cell pyroptosis and increases susceptibility on oxidative stress-induced toxicity by miR-181/SIRT1/PGC-1α/Nrf2 signaling pathway in human neuroblastoma SH-SY5Y cells: implication for association between chlorpyrifos and Parkinson's disease. *Environ Toxicol* 2019; 34: 699–707.
45 Yao B, He J, Yin X, Shi Y, Wan J, *et al*. The protective effect of lithocholic acid on the intestinal epithelial barrier is mediated by the vitamin D receptor via a SIRT1/Nrf2 and NF-κB dependent mechanism in Caco-2 cells. *Toxicol Lett* 2019; 316: 109–18.
46 Zhao X, Jin Y, Li L, Xu L, Tang Z, *et al*. MicroRNA-128-3p aggravates doxorubicin-induced liver injury by promoting oxidative stress via targeting Sirtuin-1. *Pharmacol Res* 2019; 146: 104276.

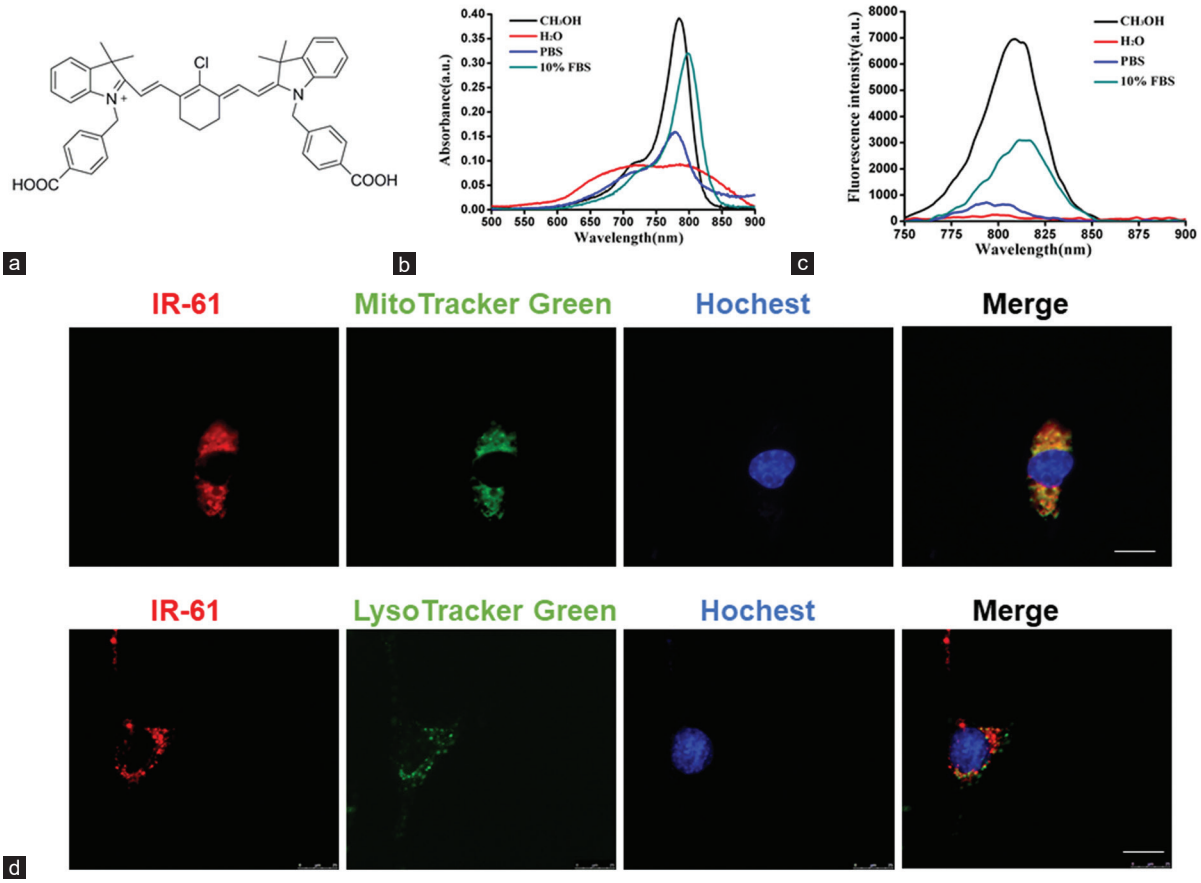

Supplementary Figure 1: Optical characterization and subcellular localization of IR-61. (**a**) Chemical structure of IR-61. (**b**) Absorption spectra and (**c**) emission spectra of IR-61 in methanol, water, PBS and 10% FBS. (**d**) Determining mitochondrial targeting of IR-61 in CCSMCs by costaining with IR-61 and MitoTracker Green or LysoTracker Green. Scale bar = 25 μm. CCSMCs: corpus cavernosum smooth muscle cells; FBS: fetal bovine serum; PBS: phosphate buffer saline.

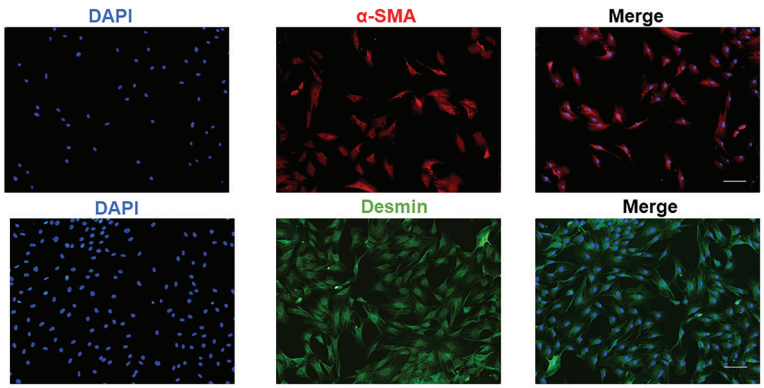

Supplementary Figure 2: Identification of cultured CCSMCs of CCSMCs. Cultured CCSMCs were identified by immunofluorescence positive for anti-Desin antibody and anti-α-SMA antibody. Scale bar = 50 μm. CCSMCs: corpus cavernosum smooth muscle cells; α-SMA: α-smooth muscle actin.

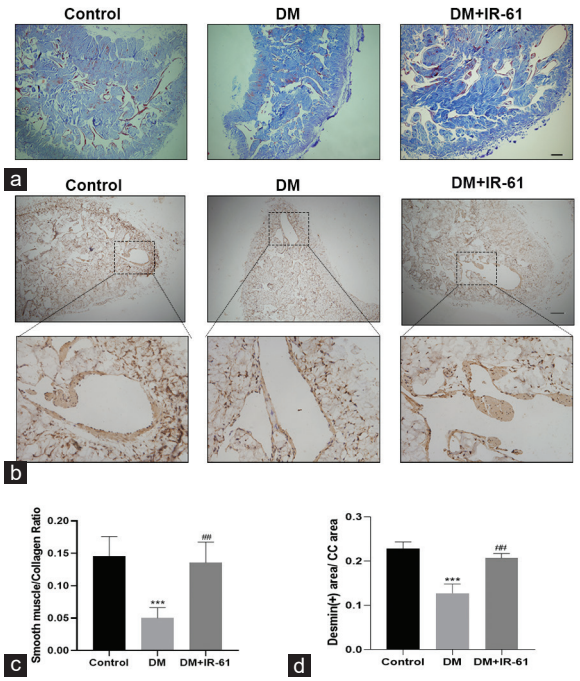

Supplementary Figure 3: IR-61 ameliorated diabetes-induced morphological changes in the corpus cavernosum. (**a**) Representative images of HE and Masson's trichrome-stained corpus cavernosum tissue in the control, DM and DM + IR-61 groups. Scale bar =100 μm. (**b**) Determination of smooth muscle content in the corpus cavernosum by immunohistochemical staining of Desmin in the control, DM and DM + IR-61 groups (n = 3 per group). (**c**) Quantification of the ratio of smooth muscle content to collagen in each group (n = 3 per group). (**d**) Quantification of the ratio of Desmin positive area in the cavernous tissue. $^{**}P < 0.01$, the indicated group compared with the Control group; $^{\#\#}P < 0.01$, the indicated group compared with the DM group.

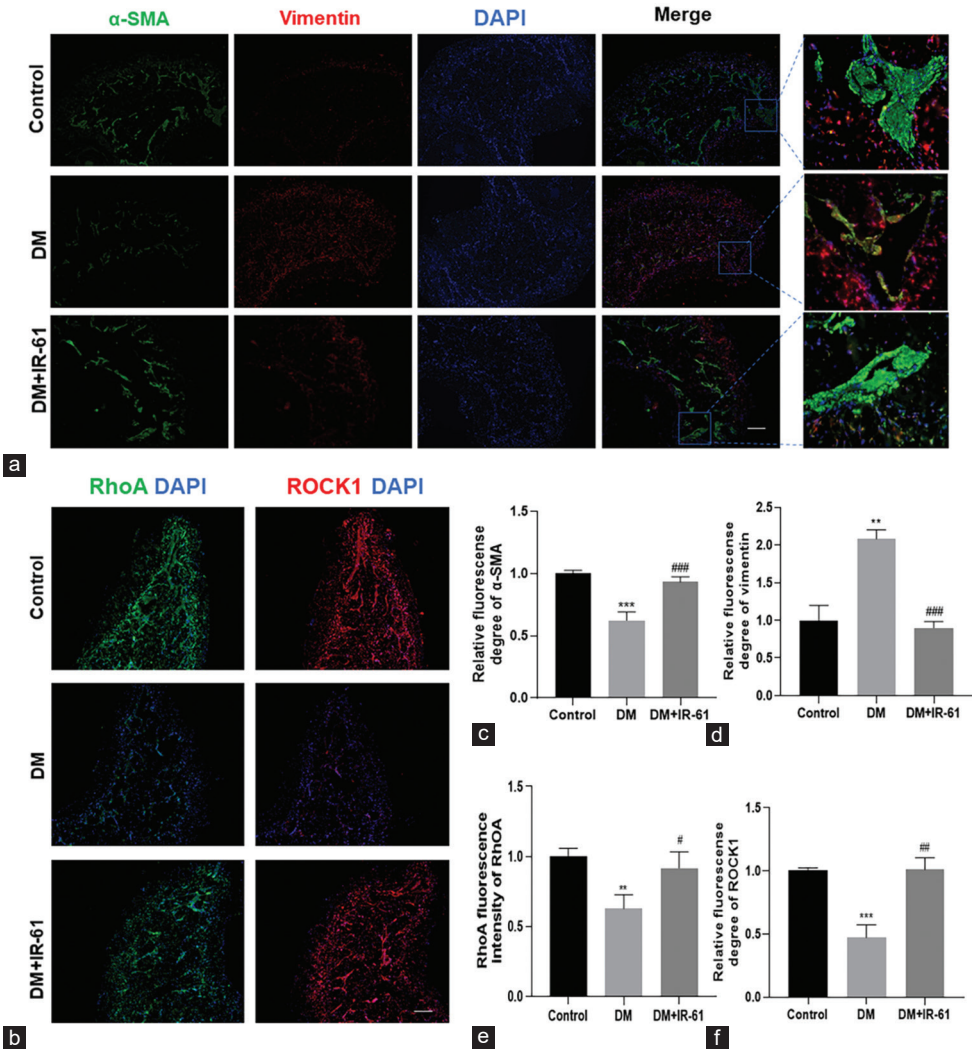

Supplementary Figure 4: IR-61 mitigated phenotypic transition of CCSMCs in diabetic rats. (**a**) Representative images of immunofluorescence costaining with α-SMA and vimentin. Scale bar = 100 μm. (**b**) Representative images of immunofluorescence staining of RhoA and ROCK1. Scale bar = 100 μm. Quantitative analysis of the fluorescence intensity of (**c**) α-SMA, (**d**) Vimentin, (**e**) RhoA and (**f**) ROCK1 ($n = 3$ per group). $^{**}P < 0.01$, the indicated group compared with the control group; $^{***}P < 0.001$, the indicated group compared with the control group; $^{\#}P < 0.05$, the indicated groupcompared with the DM group; $^{\#\#}P < 0.01$, the indicated group compared with the DM group; $^{\#\#\#}P < 0.001$, the indicated group compared with the DM group. CCSMCs: corpus cavernosum smooth muscle cells; DM: diabetes mellitus; RhoA: Ras homolog gene family, member A; ROCK1: Rho-associated, coiled-coil containing protein kinase 1; α-SMA: α-smooth muscle actin.

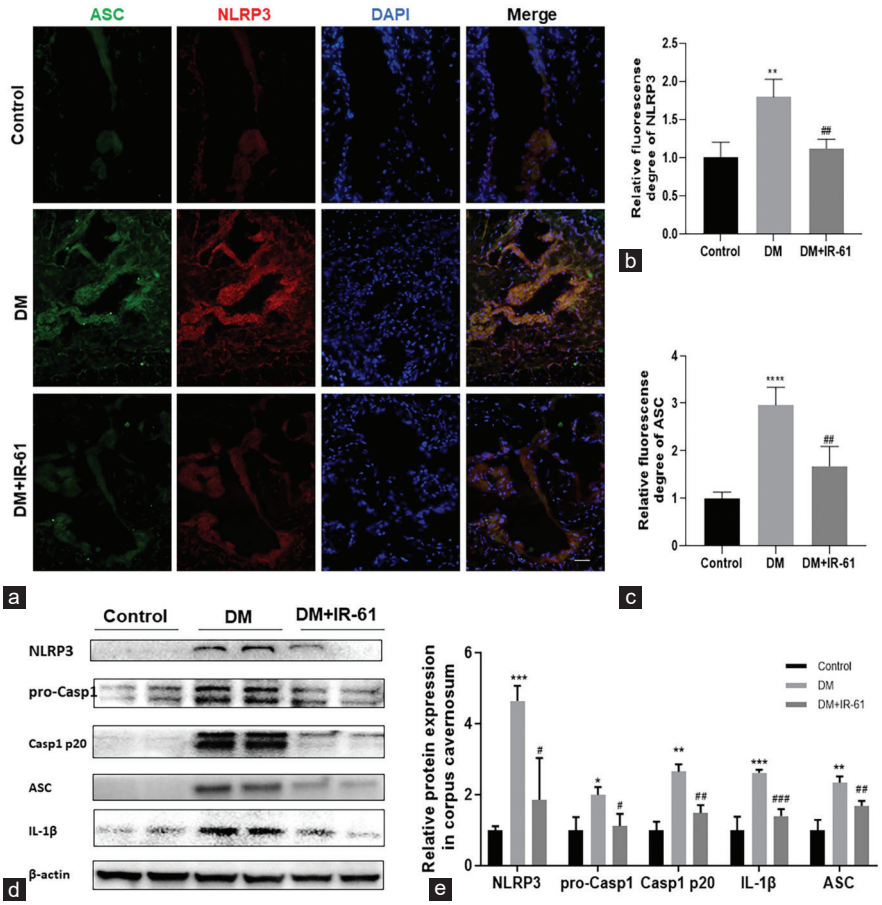

Supplementary Figure 5: IR-61 suppressed diabetes-induced inflammation and NLRP3 inflammasome activation in the corpus cavernosum. (**a**) Representative images of NLRP3 and ASC immunofluorescence staining. Quantitative analysis of the fluorescence intensity of (**b**) NLRP3 and (**c**) ASC ($n = 4$ per group). Scale bar = 20 μm. (**d**) Western blot analysis of NLRP3, pro-caspase-1, caspase-1 p20, IL-1β, and ASC in the corpus cavernosum. (**e**) Quantitative analysis of relative protein levels of NLRP3, pro-caspase-1, caspase-1 p20, IL-1β and ASC ($n = 4$ per group). $^{*}P < 0.05$, the indicated group compared with the control group; $^{**}P < 0.01$ the indicated group compared with the control group; $^{***}P < 0.001$, the indicated group compared with the control group; $^{****}P < 0.0001$, the indicated group compared with the control group; $^{\#}P < 0.05$, the indicated group compared with the DM group; $^{\#\#}P < 0.01$, the indicated group compared with the DM group; $^{\#\#\#}P < 0.001$, the indicated group compared with the DM group. NLRP3: nucleotide binding and oligomerization of domain-like receptor family pyrin domain-containing 3; ASC: apoptosis-associated speck-like protein containing caspase-recruitment domain; IL-1β: interleukin-1β; DM: diabetes mellitus.

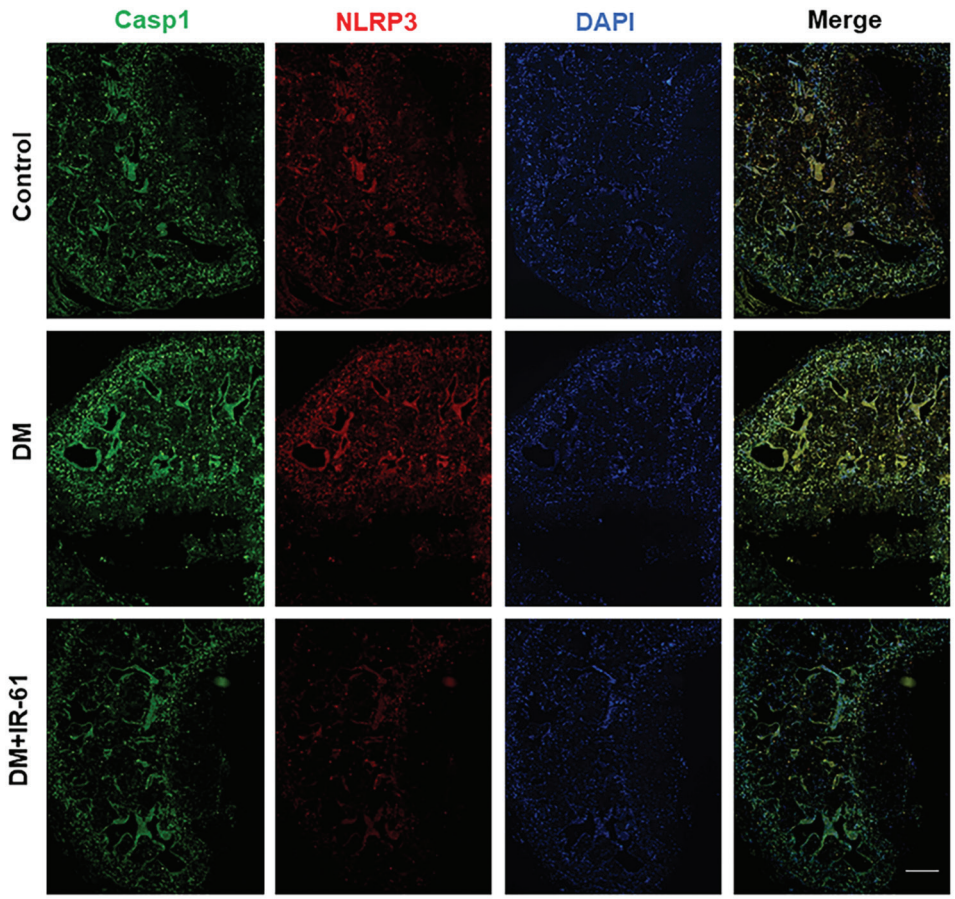

Supplementary Figure 6: IR-61 inhibited the diabetes-induced NLRP3 inflammasome activation. Immunofluorescence costaining of caspase-1 and NLRP3 confirmed that IR-61 reduced the expression of NLRP3 and caspase-1 in the penile tissues. Scale bar = 100 μm. NLRP3: nucleotide binding and oligomerization of domain-like receptor family pyrin domain-containing 3; Casp1: caspase-1; DM: diabetes mellitus.

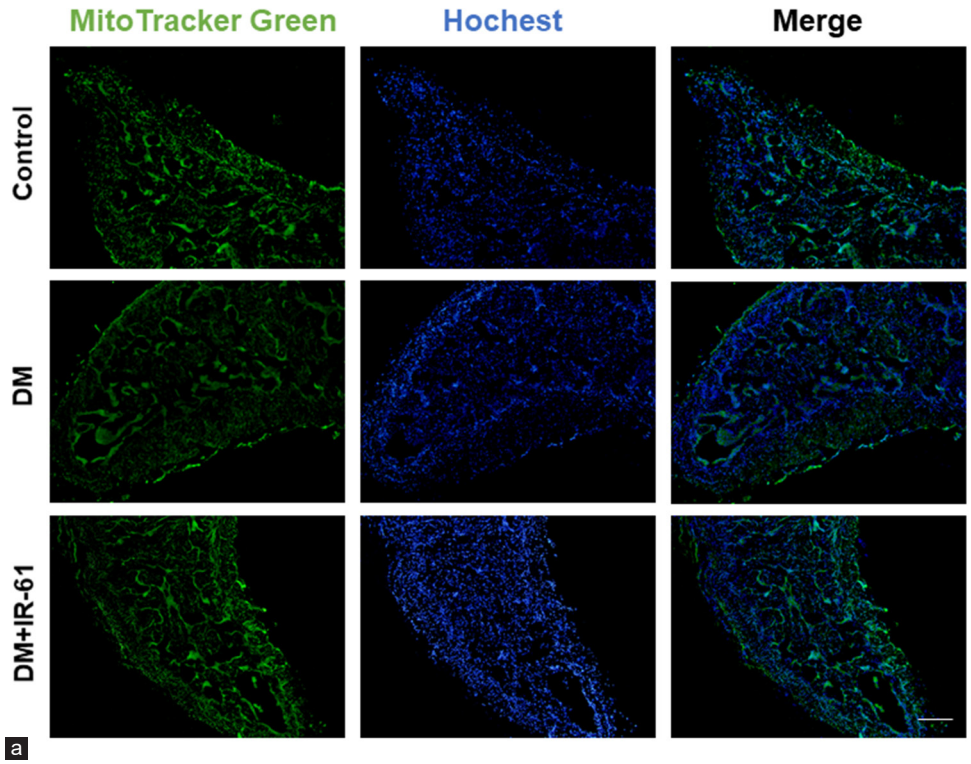

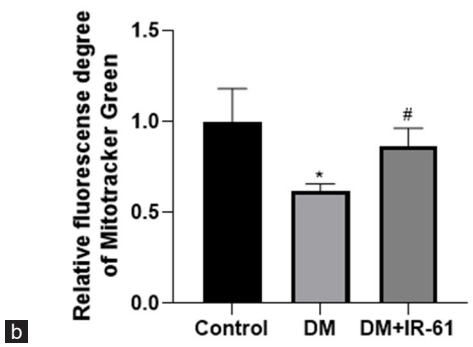

Supplementary Figure 7: IR-61 rescued the mitochondria capacity in the cavernous tissue. (**a**) Relative fluorescence staining of MitoTracker Green on fresh frozen sections of the cavernous tissue from all groups. (**b**) Quantitative analysis of MitoTracker Green fluorescence intensities of corpus cavernosum in each group (n = 4 per group). *P < 0.05, the indicated group compared with the control group; #P < 0.05, the indicated group compared with the DM group. Scale bar = 100 μm. DM: diabetes mellitus.

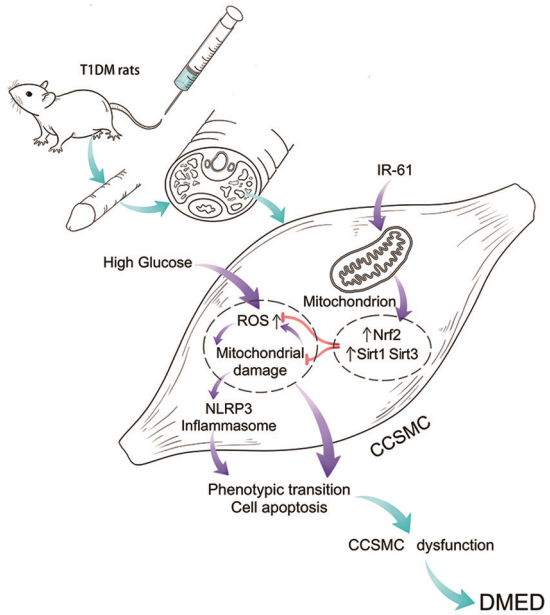

Supplementary Figure 8: Proposed schematic showing the mechanisms by which IR-61-preserved erectile function in T1DM rats. IR-61 accumulated in the cavernous tissue after intravenous injection and was located in the mitochondria of CCSMCs. IR-61 in CCSMCs increased the expression of Nrf2, SIRT1 and SIRT3, thereby decreasing mitochondrial damage and ROS production secondary to high glucose. The maintenance of mitochondrial stability and reduction in oxidative stress reduced NLRP3 inflammasome activation, apoptosis and the phenotypic transition of CCSMCs induced by diabetes, enabling IR-61 to protect the erectile function of diabetic rats by ameliorating CCSMC dysfunction. T1DM: type 1 diabetes mellitus; CCSMCs: corpus cavernosum smooth muscle cells; Nrf2: Nuclear factor (erythroid-derived 2)-like 2; SIRT1: sirtuin1; SIRT3: sirtuin3; ROS: reactive oxygen species; NLRP3: nucleotide binding and oligomerization of domain-like receptor family pyrin domain-containing 3.